Automatic Geo-location Correction of Satellite Imagery

Ozge C. Ozcanli, Yi Dong, Joseph L. Mundy
Vision Systems Inc.
Providence, RI
ozge@visionsystemsinc.com

Helen Webb, Riad Hammoud, Tom Victor
BAE Systems
Burlington, MA

Abstract

Modern satellites tag their images with geo-location information using GPS and star tracking systems. Depending on the quality of the geo-positioning equipment, geo-location errors may range from a few meters to tens of meters on the ground. At the current state of art, there is not an established method to automatically correct these errors limiting the large-scale utilization of the satellite imagery. In this paper, an automatic geo-location correction framework that corrects multiple satellite images simultaneously is presented. As a result of the proposed correction process, all the images are effectively registered to the same absolute geodetic coordinate frame. The usability and the quality of the correction framework are shown through probabilistic 3-D surface model reconstruction. The models given by original satellite geo-positioning meta-data and the corrected meta-data are compared and the quality difference is measured through an entropy-based metric applied onto the high resolution height maps given by the 3-D models. Measuring the absolute accuracy of the framework is harder due to lack of publicly available high precision ground surveys; however, the geo-location of images of exemplar satellites from different parts of the globe are corrected and the road networks given by OpenStreetMap are projected onto the images using original and corrected meta-data to show the improved quality of alignment.

Introduction

With the advancements in satellite imaging technology, there is an abundance of high resolution and high quality imagery collected on a daily basis from around the globe by many satellites. It is highly desirable to utilize these image resources to generate continuously updated high resolution digital elevation models (DEMs) for mapping, mensuration, change detection and event monitoring purposes. Many Geographic Information System (GIS) applications would also benefit greatly if existing GIS data such as road networks or building footprints could be used in conjunction with a daily stream of satellite imagery.

However, even the most modern satellite geo-positioning equipment results in varying degrees of geo-location errors on the ground, see Table 1.

Satellite	90% CE
GeoEye-1	2.5 meters
WorldView1	7.6 meters
WorldView2	12.2 meters
Quickbird	23 meters

Table 1: Geo-location accuracy of well-known satellites reported as 90% Circular Error (CE) on the ground

Figure 1: Pointing error of a satellite can be well approximated by a translation on the image plane**.**
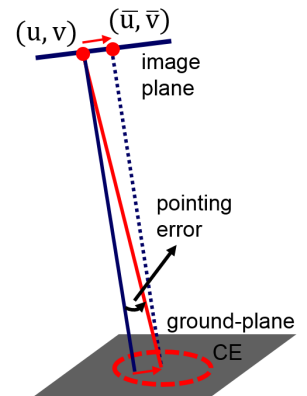
These errors need to be *relatively* corrected before the images from different satellites can be used simultaneously as part of any 3-D reconstruction algorithm since triangulation requires the rays back-projected from image features to intersect. Relative correction can be achieved by the registration of the images to a common geodetic coordinate frame which would then have a certain absolute accuracy. Absolute accuracy is critical for any application that requires GIS data, for example for road networks to align well with roads in images.
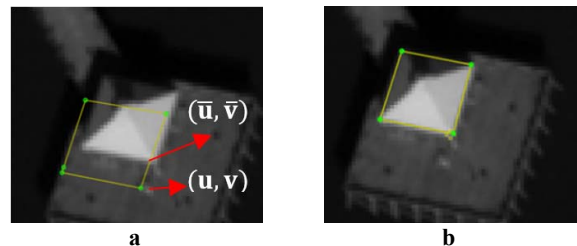

Figure 2: a) Projection of corners of a building with known geographic coordinates and elevation using the original RPC camera of the image. **b)** Projections of the same corners using the corrected RPC model.

Satellite image vendors have adopted the Rational Polynomial Coefficient (RPC) model to represent both the internal and external orientation of a satellite image in one

set of equations [1]. The RPC model provides a function that maps Earth coordinates given as (latitude, longitude, elevation) to image pixels (u, v). The function can be simplified as $u = F_{RPC}(lat, lon, elev)u_s + u_0$ and $v = F_{RPC}(lat, lon, elev)v_s + v_0$ for some scaling parameters u_s, v_s, some offset parameters u_0, v_0 and for a degree three rational polynomial function F_{RPC} with 80 coefficients. Since the satellite camera is far (typically ~500 km) from the Earth's surface, the rays for individual pixels are almost parallel to each other, as illustrated in Figure 1. Thus, geo-positioning errors can be corrected by small translations in the image plane. This type of correction is termed *bias* correction in [2] and is shown to accurately model the errors for images that are less than 50 km in size. Mathematically, the problem is to compute a correction offset, $(\Delta u_0, \Delta v_0)$, such that $\bar{u} = F_{RPC}(lat, lon, elev)u_s + u_0 + \Delta u_0$ and $\bar{v} = F_{RPC}(lat, lon, elev)v_s + v_0 + \Delta v_0$, see Figure 1 and Figure 2. Note that the correction offset geo-registers the entire satellite image over a field of view of typically 40x40 km. Depending on the geo-positioning error on the ground and the resolution of the image, the correction offsets are on the order of 5-10 pixels on the image plane. For the images collected by satellites in Table 1, the worst case correction offsets would range from 5 pixels in radius, for GeoEye-1 imagery with ~0.5 meter GSD, up to 30 pixels in radius for Quickbird imagery with ~ 1 meter GSD.
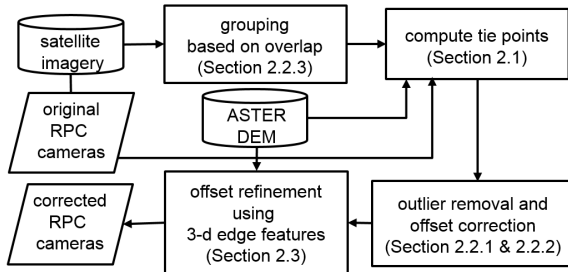

Figure 3: The process flow diagram of the proposed RPC offset correction framework.

In this paper, a bias correction framework is presented that inputs a set of multi-view satellite images with varying geo-positioning errors and registers them to a common absolute geodetic coordinate frame. First, the images are grouped according to degree of overlapping views and a correction offset, $(\Delta u_0, \Delta v_0)$, is computed for each image in each group using image-to-image correspondences and a bundle adjustment type correction algorithm, described in Section 1.4.2. Second, the offsets are refined utilizing a 3-D edge modeling framework [3] which provides denser feature registration by reconstructing contours of the buildings, roads and other structures that are visible in all the images and contribute to the 3-D model. Figure 3 shows the process flow diagram for the proposed RPC offset correction framework. Specifically, the contribution of the paper is a

system for *automatically* correcting hundreds of satellite images (each with ~40Kx40K pixels) with varying geo-location errors and bring the overall geo-location accuracy to the accuracy of the best satellite. Section 2.3 presents a novel relative correction algorithm which is used to turn semi-supervised 3-d edge based geo-correction algorithm of [3] into a completely unsupervised algorithm. Section 2.3 explains how the unsupervised 3-d edge based geo-correction algorithm is used in a consensus building framework to minimize the risk of computing a wrong offset for a given image.

1.1. 3-D modeling using satellite imagery

In this paper, a probabilistic 3-D modeling application using multi-view satellite imagery [3] is chosen as a use-case for the proposed offset correction algorithm. This algorithm represents the 3-D volume of a scene using a regular grid of cubic volume elements, *voxels*, e.g. of size 1 m³, and computes a surface occlusion probability and a surface appearance model for each voxel in the volume. The rays from the available images are cast into the volume using the images' camera models and the surface existence probabilities are updated simultaneously with their appearance models using the appearance of the rays. It is shown that the algorithm converges to the correct 3-D surface model as more images are used to update the model [3]. The critical assumption is that the geo-positioning errors of the input images are *relatively* corrected such that the triangulation errors can be absorbed within a voxel. For example, for voxels of 1 m³, a circular error (CE) of 1 meter on the ground needs to be achieved for all the input images. If the images are not adequately corrected then the rays of image pixels do not intersect at the correct voxels and the 3-D surfaces can no longer be accurately recovered. As the relative errors get more severe, the 3-D model surface heights (Z coordinate) become noisier. In this paper, the noise level in the orthographic height maps given by these volumetric 3-D models is measured to show the quality of the proposed relative registration framework.

When the relative geo-positioning accuracy of the input images is high, the 3-D surface geometry is accurately recovered in the common geographic coordinate frame induced by the input images. Any absolute error in the common coordinate frame of the input images is inherited by the geo-position of the resulting 3-D surface model. In other words, the recovered surface geometry is relatively correct but may require a global translation to remove any absolute geo-positioning error. In this paper, the improvement in the absolute accuracy of the input RPC models is demonstrated through the projections of OpenStreetMap roads and buildings onto images using the original and corrected RPC models of the images.

1.2. Related Work

Using the bias error model and a bundle adjustment algorithm, only a few ground control points are shown to reduce the geo-positioning errors down to sub-meter accuracy [4]. The critical factor is the precision of the 3-D survey positions and the 2-d image measurements, termed as *tie points*, of the ground control points. In [2], it is shown that only 2-d measurements are sufficient to correct the bias error using a block adjustment algorithm, given enough tie points. The challenge for automatic RPC correction is then the computation of these tie points as correct and well localized image-to-image correspondences. There is previous work [5,6] using sparse features such as SIFT computed from in-track stereo satellite imagery to automatically create many tie points and then remove the outliers via a RANSAC procedure. However, in this paper the input satellite imagery is assumed to come from different satellites and collected at different times, months or years apart. Computing tie points from such imagery automatically is more challenging due to illumination changes, seasonal and atmospheric appearance differences, occlusions and parallax effects of tall buildings when projected with very different viewpoints. The algorithm proposed in this paper (Section 2.1) successfully computes a rich set of tie points for groups of images with significant collection time differences and coming from different satellites, without a priori ground control points.

A major approach is to compute tie points between satellite images and DEMs [5] or renderings from DEMs [7], and use these tie points to correct the bias error. However, this line of work inherits the absolute and relative inaccuracy of DEMs as well as the errors introduced by resolution and surface geometry mismatches between the satellite images and the terrain-only DEMs. In this paper, tie points are computed only between images and thus any inaccuracy due to DEMs is avoided[1].

Geo-location correction

The proposed RPC camera offset correction framework is comprised of three major algorithmic components: 1) sparse image-to-image correspondence computation for a group of images; 2) offset correction of a group of images using a set of correspondences and 3) offset refinement/computation of an image using a 3-D edge model. The process flow diagram of the proposed framework using these algorithmic components is shown in Figure 3 and each component will be explained in the following sections. The first two components automatically generate tie points and reduce the errors

[1]Note that in this paper, ASTER DEM tiles (30 meter resolution) are also used albeit only to set reasonable estimates for minimum and maximum elevations in a given area and to provide a rough ground plane to constrain the search for registration.

down to positioning accuracy of the correct tie points, then the edge modeling framework refine the offsets and bring the errors down to the level of edge model resolution. Note that edge modeling is also capable of correcting bias when the original cameras of the images are passed to it given that the edge model has been updated with 5-10 corrected images. This correction capability is used for images that do not form enough tie points with other images to support bundle adjustment. However the edge alignment search radius is increased to insure that the global minimum is obtained.
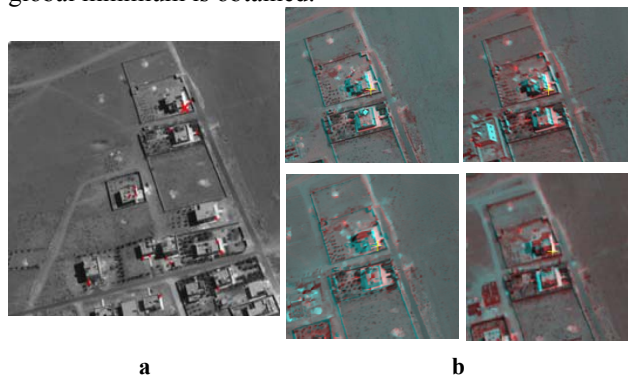

a   **b**

Figure 4: a) A base image patch with detected Harris corners (red points). **b)** Alignment of patches from other images in the group on the base patch around a selected correspondence point (marked with yellow plus sign). The base patch is shown in the red channel and the aligned patches are shown in the green and blue (cyan) channels.

1.3. Image-to-image correspondence computation

Given a group of satellite images, the area of overlap (intersection) between the input images is computed using the footprints of the images given in the meta-data, see Figure 5a. One of the images in the group is selected as the base image and the intersection area in this image is regularly cropped into smaller image patches corresponding to sizes of roughly 250 meter by 250 meter on the ground, Figure 4a. The Harris corner detection algorithm is then run on each base patch to generate a sparse set of potential correspondences from each patch, Figure 4a. Given a base image patch, it is possible to roughly align patches from the other images that geographically correspond to this same area using the RPC models of the images and a digital elevation model (DEM) as a rough ground plane. Specifically, the corresponding image patch from the second image is first ortho-rectified [1] and then projected back onto the base patch using the base image's RPC model. Depending on the geo-positioning errors of the RPC models of the images and the DEM ground plane accuracy, the alignment error can be 10s of pixels; however, the RPC model provides an adequate initial alignment. This initial alignment is corrected using an enhanced phase correlation (EPC) algorithm [8] around each corner point and at multiple

scales across all images to account for resolution differences. The corners that generate correlation peaks and satisfy a threshold requirement are returned as the image-to-image correspondences for the patch. Figure 4b shows the final alignment of the patches from four other images in the group relative to the base patch around a selected correspondence point. Observe that the correspondence point is well localized in all images at the correct corner of the corresponding building structure.

EPC successfully avoids erroneous correspondences from cloudy regions and is robust to the illumination differences and parallax effects among the images. When the computed correspondences are semantically correct, i.e. when they come from a common 3-D feature point, the localization errors are observed to be within two pixels. The two pixel error is not sufficiently accurate for 3-D reconstruction and must be further refined (Section 2.3); however, it is good enough to be used as part of a bundle adjustment type bias correction algorithm as described in the next section (Section 2.2). It is observed that the proposed algorithm can generate wrong correspondences due to moving objects, vegetation or changes in the structure of the objects in the scene, e.g. construction sites.
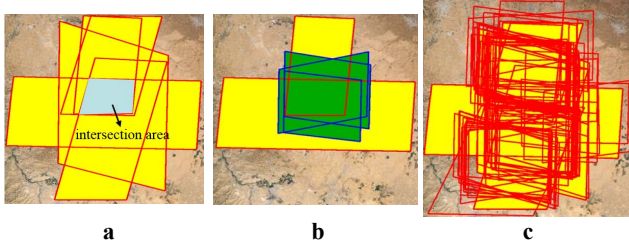

a **b** **c**

Figure 5: a) Footprints of 6 GeoEye-1 images selected as a seed group. **b)** Footprints of the images in the second group to be corrected using 2 seeds. **c)** Footprints of all the images that are corrected

1.4. RPC offset correction

Given a group of satellite images, and a set of image-to-image correspondences, a random sample consensus (RANSAC) procedure is used to first eliminate wrong correspondences. The initial algorithm in this RANSAC procedure computes a correction offset for each image in the group using one image-to-image correspondence only, Section 1.4.1. The distances between the correction offsets given by different correspondences are computed in the image domain and the correspondences that yield less than 2 pixel difference are selected as inliers. The inlier correspondences participate in the second algorithm, Section 1.4.2, which refines the offsets through bundle adjustment using all the correspondences at the same time.

1.4.1 *Offset correction using one image-to-image correspondence*

Using the RPC model of a satellite image, it is possible

to back-project a ray from any image point (u, v) onto a horizontal plane with a given elevation, Z, and compute a 3-D point (X, Y, Z) as the intersection point of the ray with the plane [9]. In the proposed correction scheme, given a group of images, and image-to-image correspondences, a ray from each image-to-image correspondence point is cast onto a series of horizontal planes with elevations in the range $[Z_{min}, Z_{max}]$ and with ΔZ increments[2], see Figure 6. For each plane, $z = Z_i$, a set of points on the plane $\{(X_i^j, Y_i^j)\}$ are generated for each image j. A weighted mean $(\widehat{X}_i, \widehat{Y}_i)$, and a weighted scatter value, σ_i, is computed as $(\widehat{X}_i, \widehat{Y}_i) = (\sum_j w_j X_i^j, \sum_j w_j Y_i^j)$ and

$$\sigma_i = \sqrt{\sum_j w_j (X_i^j - \widehat{X}_i)^2 + \sum_j w_j (Y_i^j - \widehat{Y}_i)^2}$$

where the weights for each image are given such that $\sum_j w_j = 1$. The purpose of weighting is to reflect the relative reliability of the RPC camera model of an image and is explained in Section 1.4.3. The mean position is the estimate of the 3-D intersection point at the corresponding plane elevation and the scatter value measures the accuracy of ray intersection for this 3-D point. Observe from Figure 6 that the scatter value is minimized around the correct elevation of the 3-D intersection point induced by this image-to-image correspondence. The elevation with the minimum scatter, $\widehat{Z}$ in Figure 6, is chosen as the elevation of the 3-D intersection point of the image-to-image correspondences. The 3-D intersection point of this best z value, $(\widehat{X}, \widehat{Y}, \widehat{Z})$, can then be projected back to the images using the RPC models to get $(\hat{u}_j, \hat{v}_j)$ for image j and the correction offsets are computed as $(\Delta u_0^j, \Delta v_0^j) = (\hat{u}_j - u_j, \hat{v}_j - v_j)$ for each image. Also observe from Figure 6 that by using the known ray geometry in 3-D, parallax effects are automatically taken into account.
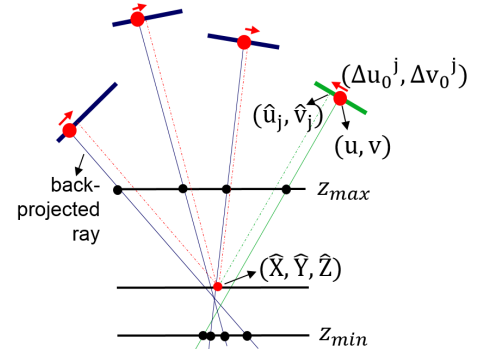

Figure 6: Offset correction using an optimal estimate for a common 3-D intersection point given a group of satellite images and one image-to-image correspondence as explained in Section 1.4.1.

The proposed algorithm ensures that the images in the

---

[2] A viable range for Z values, $[Z_{min}, Z_{max}]$, is retrieved from the image meta-data.

group have zero *relative* pointing error as their rays are moved to intersect *perfectly* at the correspondence point. However, the *absolute* accuracy of the correction depends on the absolute accuracy of the recovered 3-D intersection point. Observe from Figure 1 that, assuming the pointing errors of the rays are unbiased, their projected distribution on a plane can be well approximated by a normal distribution with zero mean. If it is assumed that on the correct elevation plane, the $\{(X_i^j, Y_i^j)\}$ values are distributed normally with zero mean around the correct absolute position $(\overline{X}, \overline{Y})$, then as $j \to \infty$, the mean value $(\widehat{X}_i, \widehat{Y}_i)$ will approach $(\overline{X}, \overline{Y})$. Thus, the proposed algorithm approaches better absolute accuracy as the number of images in the group is increased. In practice, groups of as few as 5 images are found to achieve adequate absolute accuracy for the GeoEye-1 imagery used in the experiments for this paper.
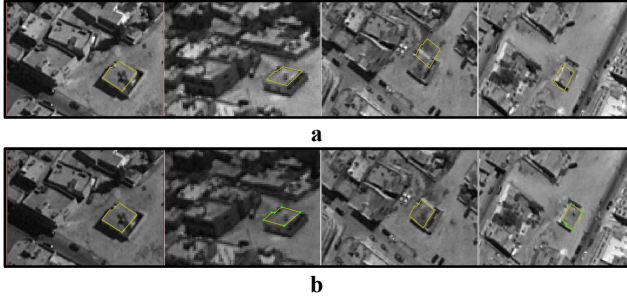

a

b

Figure 7: Projections of the rooftop (shown in yellow lines) of a building using **a)** original RPC cameras **b)** corrected RPC cameras of a group of 4 images.

1.4.2   Offset correction using multiple image-to-image correspondences

Given a group of images and a set of inlier correspondences which generate consistent global offsets for the images, the offsets are refined using a bundle adjustment framework where the 3-D intersection points are refined simultaneously with the camera correction offsets. Mathematically, the following reprojection error is minimized using the Levenberg-Marquardt optimization algorithm:

$$\sum_{k=1}^{M} \sum_j [\left(U_{RPC}^j(\widehat{X}_k, \widehat{Y}_k, \widehat{Z}_k; \Delta u_0{}^j), V_{RPC}^j(\widehat{X}_k, \widehat{Y}_k, \widehat{Z}_k; \Delta v_0{}^j) \right) - (u_j, v_j)_k]$$

where $(u_j, v_j)_k$ is the jth image coordinate of the kth image-to-image correspondence, $(\widehat{X}_k, \widehat{Y}_k, \widehat{Z}_k)$ is the current 3-D intersection point of the kth correspondence and the current offset of jth image $(\Delta u_0{}^j, \Delta v_0{}^j)$ is fixed across the correspondences. The 3-D intersection points are initialized using the algorithm described in Section 1.4.1 for each image-to-image correspondence and the camera offsets $(\Delta u_0{}^j, \Delta v_0{}^j)$ are initialized with the values given by

one of the inlier correspondences. Figure 7 shows a group of 4 GeoEye-1 images and the projections of the corners of a building with known height onto each image with the original and the corrected RPC models.
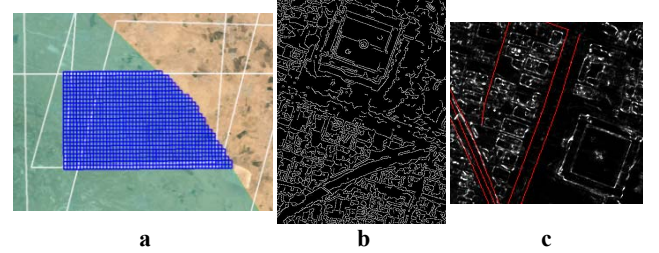

a   **b**   **c**

Figure 8: a) The 400 m x 400 m scene volumes initialized at the intersection area of the seed images shown in Figure 5a. **b)** An example edge image used in updating the 3-D edge model. **c)** An orthographic projection of the 3-D edge features of a model updated with 40 edge images with corrected RPC models. Red lines show the projections of OpenStreetMap roads onto the orthographic expected edge image to demonstrate the absolute accuracy of the input corrected RPC cameras.

1.4.3   Grouping images and selection of seed group

Given a set of images to correct with varying geo-positioning errors and resolution, it is difficult to find mutual correspondences among all the images. The reason is that the overlap area gets smaller as more images are used, and varying resolution and cloud coverage across images makes it difficult to find good correspondences. In practice, it is easier to generate groups of 3-10 images with a good correspondence set. One strategy is to group all the images into groups with 3-10 images and run the group correction algorithm independently on each group; however, the global accuracy of each group depends on the geo-positioning errors of the members of each group and may vary from group to group resulting in relative geo-location inconsistency among the groups. A better strategy is to generate a *seed group* from images with best resolution and smallest geo-positioning errors to establish a coordinate frame with best possible absolute accuracy, see Figure 5a. This seed group is corrected first using the group correction algorithm (Sections 1.4.1 and 1.4.2) where the weights of all images in the group are set to be equal. Then a second group of 3-10 images is formed where 2 images come from the seed group, Figure 5b. The weights of the seed images in this group are set to 0.5 and the weights of the other images are set to 0. With this weight setting, 3-D intersection points during group correction procedure are entirely determined by the two seed images in the group, effectively registering the other images in this group to the seed's absolute coordinate frame. Then a third group is formed and so on. All the rest of the images can be grouped in this manner such that two images are already corrected and then sequentially corrected group by group. Figure 5c shows footprints of 100 images that are corrected starting from the initial 6

seed images. Observe that the coverage area of images with geo-locations corrected to a common absolute coordinate frame increase beyond the initial seed coverage and new images that intersect with this larger area can now be corrected using the same group-and-correct algorithm. Geographically distant areas can be corrected using different seed groups and growing the geo-located images around them if enough images to connect to them cannot be found.
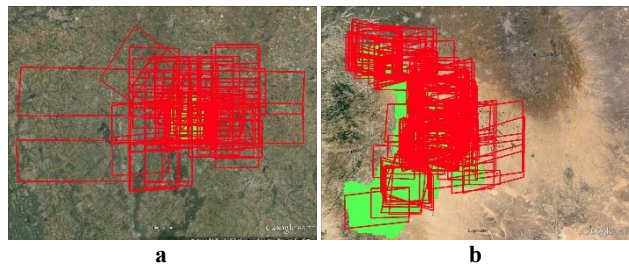

| a | b |

Figure 9: Footprints of all the satellite images used in the experiments in this paper collected over **a**) India and **b**) Jordan regions by GeoEye1, Worldview1, Worldview2, Quickbird satellites over a period of 5 years.

1.5. Offset refinement/correction via 3-D edge modeling

The absolute accuracy of the corrected geo-locations of imagery using the framework of Section 2.2 depends on the quality of the image-to-image correspondences given by the algorithm described in Section 2.1. The wrong correspondences are discarded with the RANSAC framework; however, the inlier correspondences may still have localization errors up to 2 pixels. In practice, a second round of refinement using a 3-D edge model [10] is found to be necessary to ensure that all the images are relatively corrected to a level determined by the voxel resolution of the model.

The 3-D edge models are volumetric models as in [3] and are updated with edges computed from the input satellite images instead of image intensity, Figure 8b. The details of the update equations are given in [10] but essentially every voxel in the 3-D scene volume stores an edge existence probability which converges to 1 as more image rays contribute with an edge ray piercing that voxel. In [10], a semi-supervised bias correction algorithm is presented where the 3-D edge model is initialized with a set of *seed* images which are *manually* corrected. Then the rest of the images are aligned by correlation to the projections of the 3-D edge features in the current model onto the input image. In this paper, the same edge correlation based correction algorithm is used but the bias correction of the *seed* images is automated using the algorithms described in Sections 1.4.1 and 1.4.2. The final absolute accuracy is typically better than the seed accuracy due to the averaging effect of the edge accumulation in each voxel. Figure 8c shows orthographic projections of 3-

D edge features recovered using this correct-and-update algorithm. Observe that most of the building roof contours are recovered along with some road features. OpenStreetMap roads (in red) are projected onto this edge image to show the final absolute accuracy of the model.
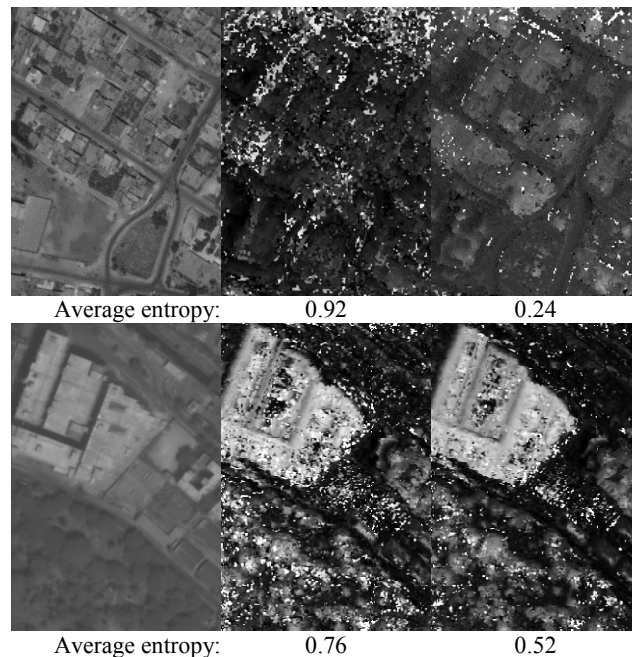

| Average entropy: | 0.92 | 0.24 |

| Average entropy: | 0.76 | 0.52 |

Figure 10: Orthographic height maps given by 3-D models after 40 image updates. The first column shows an example (cropped) input image for the scene, the second column shows a height map given by a model using original RPC cameras of the input images and the last column shows when the input cameras are corrected by the proposed framework. Observe from the last column that the streets, building shapes and the tree heights are recovered better with the corrected cameras.

The 3-D edge model volumes are initialized to have 1 m^3 voxel resolution and 400x400 m^2 local horizontal span to minimize Earth's curvature effects during reconstruction, Figure 8a. The heights of the 3-D edge model volumes are initialized using ASTER DEM tiles of the area with 80 meter margin added on top of the highest terrain elevation to account for buildings. The quality of the edge-based corrections vary depending on the presence of surfaces in the scene that can generate a set of edges. However, note that the satellite images have swath width of ~50 km and one image intersects many much smaller 3-D volumes, Figure 8a. In this paper, a RANSAC procedure is proposed to correct the bias errors of a given image using all the 3-D edge models that intersect it. In order to correct an image, a consensus among the models is sought and the correction offset of the inlier model with the largest consensus is selected. The 3-D edge models are initialized on the intersection area of the seed images given by Section 1.4.3, Figure 8a, and these seed images with corrected cameras are used to update the model.

Given a non-seed image, if it was already corrected by the algorithm in Section 1.4.3, then the search space of edge image correlation is significantly reduced and its offset is refined by the consensus amount given by all the scenes. In practice correction offsets are only refined by a few pixels. Given a non-seed image which was *not* corrected by the algorithm in Section 1.4.3 (e.g. due to lack of enough tie points to any of the groups), then the search space of edge image correlation is set according to the geo-positioning error of the satellite and its correction offset is similarly set by the consensus amount given by all the scenes. In both situations, the final absolute accuracy of a corrected image is the same as the accuracy of the corrected seed imagery. Note that this final stage is capable of geo-correcting images using only a handful of automatically corrected seed imagery. However, grouping and relatively correcting imagery as described in Section 2.2.3 is beneficial as it reduces the search space of the 3-d edge based correction.
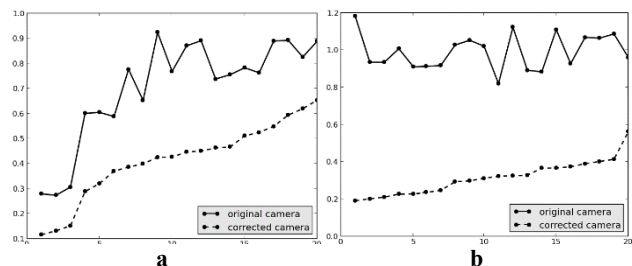

Figure 11: A plot showing average entropy values (y axis) for 20 randomly selected scenes in **a)** India and **b)** Jordan regions.

Experiments and Results

For the experiments in this paper, two geographic areas in Jordan and India are selected with roughly 200 satellite resources in each region, Figure 9, with images from GeoEye1, Worldview1, Worldview2 and Quickbird satellites.

Both regions have high to medium urban coverage that enables computation of a rich set of image-to-image correspondences and edge features for refinement. All the images are run through the proposed bias correction system of Section 2 where the seed groups are selected among GeoEye-1 imagery for best possible absolute accuracy, see Table 1. The system computes an offset successfully for 67% of the images. The failure cases are due to lack of sufficient tie points and/or lack of consensus during 3-D edge feature based refinement/correction and caused by clouds or haze in the images. The uncorrected images are discarded by the system. The relative accuracy of the corrected images are verified by manually labeling one selected building (as in Figure 7) and the projection errors are found to be less than 1 pixel for each image.

For further evaluation of the bias corrections, the 3-D scene modeling framework of [3,10] is used with 400x400x100 m³ scene volumes of 1 m³ voxel resolution.

The reduction in the noise level of the output models are measured when the models are built by the original RPC cameras vs. the corrected RPC cameras of the same input images. A volumetric 3-D model usually needs around 40 image updates to converge and so the scenes are updated with at least 40 images.
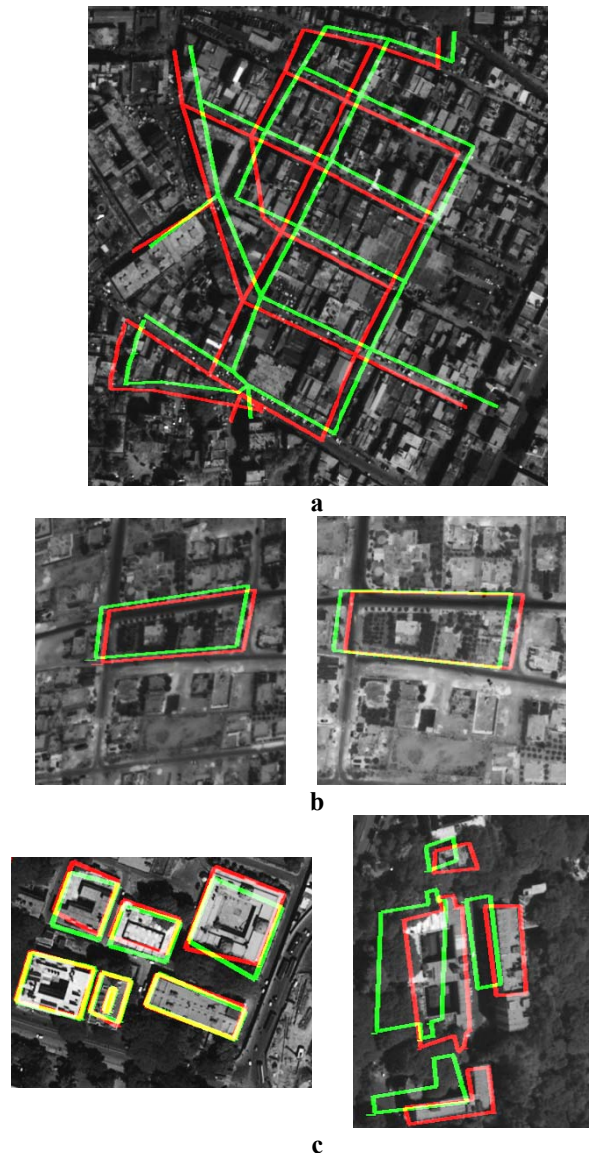

Figure 12: Projections of OpenStreetMap roads onto **a)** a Quickbird image over India region **b)** two Worldview2 images over Jordan region using their bias corrected cameras. **c)** Projections of building footprints given by OpenStreetMap over India region (the original projection is shown in green and the projection with corrected cameras is shown in red).

The resulting orthographic height maps of the recovered 3-D surfaces are dramatically different depending on the initial errors of the input images. Figure 10 shows two example scenes from both regions and their height maps with original and corrected cameras. The noise level in

these height maps are measured as the average entropy of 2 meter by 2 meter patches in the height map. The entropy value depends on the observed structure in the patch, for example flat areas have entropy close to zero, while vegetation patches give values around 2. Completely random patches have entropy value 8 with 256 possible height values (the absolute height maps are shifted to 0,255 range such that each increment is 1 meter). The actual value of the average entropy of a height map varies depending on the scene content; however, it is expected that the average entropy will be reduced significantly when the models converge to less noisy surfaces with bias corrected cameras. Observe from Figure 10 that this result is indeed the case for both examples. Figure 11 shows a plot of the average entropy values for 20 randomly selected scenes in the areas covered by the corrected satellite resources of Figure 9, significant reductions in entropy are observed for all of them.

The entropy measure demonstrates the relative accuracy of the bias corrected cameras. The absolute accuracy of the proposed framework can be demonstrated by projecting roads and building footprints given by any GIS resource. In this paper the publicly available OpenStreetMap database is used for this purpose. Figure 12a,b show projections of roads onto images with large bias corrections. Note that OpenStreetMap accuracy depends on the accuracy of the GPS equipment used by the contributor of the data points so it is not realistic to expect exact alignment of these features; however, the alignments are much improved when the bias corrected cameras are used.

For the building projections, the height maps given by the 3-D models are used with the bias corrected cameras. The alignments are compared to the projections using ASTER DEM elevations and original RPC models. It can be observed from Figure 12c that the footprints given by bias corrected cameras align better with the roof-tops of the corresponding buildings when bias corrected RPC models are used. It should also be observed that the projections differ more significantly as the building height increases since better elevation estimates are given by the 3-D surface model as compared to ASTER DEM.

Conclusions

A fully automated registration framework is presented to align multiple satellite images simultaneously to a common absolute coordinate frame. The framework corrects imagery from different satellites with varying degrees of geo-positioning errors. The absolute accuracy of the final alignment is bounded by the geo-positioning errors of the seed group. For the experiments in this paper, Geo-Eye1 images are selected to form seed groups, yielding less than 2.5 meter absolute error which is demonstrated by the betterment in the alignments of OSM roads when projected onto the corrected imagery. The

relative accuracy of registration to a common coordinate system is proven through the improvement of the triangulation accuracy of scene surfaces as part of a 3-D modeling framework, when the corrected RPC camera models of the images are used.

References

[1] G Dial and J Grodecki, "RPC replacacement camera models," in *Proceedings of the ASPRS 2005 Annual Conference*, 2005.

[2] Jacek Grodecki and Gene Dial, "Block Adjustment of High-resolution satellite images described by Rational Polynomials," *Photogrammetric Engineering and Remote Sensing*, vol. 69, pp. 59-68, 2003.

[3] Thomas Pollard and Joseph L Mundy, "Change Detection in a 3-D World," in *Proc. of Computer Vision and Pattern Recognition (CVPR)*, 2007.

[4] Clive S Fraser and Harry B Hanley, "Bias compensation in rational functions for IKONOS satellite imagery," *Photogrammetric Engineering and Remote Sensing*, vol. 69, pp. 53-58, 2003.

[5] Pablo d'Angelo and Peter Reinartz, "DSM based orientation of large stereo satellite image blocks.," *Int. Arch. Photogrammetry and Remote Sensing Spatial Inf. Sci*, vol. 39, pp. 209-214, 2012.

[6] Jaehong Oh, Charles Toth, and Dorota Grejner-Brzezinska, "Automatic Georeferencing of Aerial Images Using High-resolution stereo satellite images," in *ASPRS Annual Conference*, 2010.

[7] Mark D Pritt and Kevin J LaTourette, "Automated Georegistration of Motion Imagery," in *Applied Imagery Pattern Recognition Workshop (AIPR)*, 2011.

[8] Victor Tom, G K Wallace, and G J Wolfe, "Image registration by a statistical method," in *Proc. SPIE Applications of Digital Image Processing VI*, vol. 432, 1983.

[9] Edward M Mikhail, James S Bethel, and J C McGlone, *Introduction to Modern Photogrammetry*.: John Wiley & Sons, Inc., 2001.

[10] Thomas Pollard, Ibrahim Eden, Joseph L Mundy, and David B Cooper, "A Volumetric Approach to Change Detection in Satellite Images," *ASPRS Photogrammetric Engineering & Remote Sensing Journal*, vol. 76, no. 7, pp. 817-831, 2010